

RESEARCH ARTICLE

Agricultural Vehicle Automatic Navigation Positioning and Obstacle Avoidance Technology Based on ICP

NING XU^{1,2,3}, ZHIHE LI¹, JIANMING KANG^{2,3}, QINGSHAN MENG^{2,3}, AND MENG MENG NIU^{2,3}¹College of Agricultural Engineering and Food Science, Shandong University of Technology, Zibo 255000, China²Shandong Academy of Agricultural Machinery Sciences, Jinan 252100, China³Huang Huai Hai Key Laboratory of Modern Agricultural Equipment, Ministry of Agriculture and Rural Affairs, Jinan 250100, China

Corresponding author: Zhihe Li (lzh_0533@163.com)


This work was supported in part by Shandong Province Key Research and Development Plan (Major Science and Technology Innovation Project): Research and Application of Intelligent Agricultural Equipment for Hilly and Mountainous Areas under Grant 2022CXGC020706, and in part by Shandong Province Lu-Yu Science and Technology Cooperation Project: Application Demonstration of Intelligent Weeding Technology and Equipment in Mountain Orchard under Grant 2023LYXZ018.

ABSTRACT The problem of closed branches and leaves in orchards can cause satellite navigation systems to experience star loss, leading to safety issues such as collisions and loss of control. To address this issue, this study develops a multi-mode navigation control system for satellite navigation and sensor tracking, aiming to achieve multi-mode intelligent path judgment and ensure the accuracy and safety of operations. This method utilizes point cloud iterative nearest point algorithm LiDAR technology to gain 3D information of the surrounding environment when satellite signals are unavailable. Through perception and analysis of the environment, real-time path planning and obstacle avoidance decision-making are achieved. At the same time, through micro-inertial navigation technology, accurate perception and control of the position and attitude of navigation equipment are achieved, thereby achieving precise control of the operation process. According to relevant experimental data, the experimental distance accuracy based on the vehicle mounted daytime environment dataset was 84.88%, and the duration accuracy was 97.63%. Accordingly, the proposed system is capable of accurately determining the current position and heading, as well as making path planning and obstacle avoidance decisions based on real-time environmental information. This ensures the accuracy and safety of operations. The research method exhibits higher stability and reliability in orchard operations, providing an effective solution for the accuracy and safety of orchard operations.

INDEX TERMS Point cloud iteration nearest point algorithm, agricultural vehicles, automatic navigation and positioning, obstacle avoidance technology, scale invariant feature transformation.

I. INTRODUCTION

The accelerated advancement of contemporary agricultural techniques has rendered the precise positioning and secure avoidance of obstacles by agricultural vehicles a pivotal component in the overall process of agricultural production [1]. Agricultural vehicles need to face various complex and ever-changing terrains and environments during their journey in the fields. Especially in orchard operating environments, the problem of canopy closure of branches and leaves

The associate editor coordinating the review of this manuscript and approving it for publication was Tariq Umer .

can seriously affect the signal reception of satellite navigation systems, making it easy to experience star loss. This will also to some extent affect the precise navigation of agricultural vehicles, and may even cause problems such as vehicle collisions and loss of control [2], [3]. Therefore, how to accurately and effectively achieve Automatic Navigation and Positioning (ANP) and obstacle avoidance for agricultural vehicles has a decisive impact on agricultural production efficiency and safety [4]. The principal limitation of existing agricultural navigation technology is its inadequate adaptability to complex environments. This can readily result in a reduction in positioning accuracy and stability in situations such as

signal occlusion and multi-path interference [5]. Therefore, there is an urgent need to innovate and optimize navigation technology, enhance its adaptability in changing environments, and ensure the accuracy and reliability of navigation. To improve the accuracy of vehicle navigation, F Aghaei et al. used ray tracing technology for channel modeling based on vehicle positioning systems, and considered multiple frequencies and transmitter types. Furthermore, the research demonstrated that ray tracing simulation could consider the propagation environment for three-dimensional modeling. This approach allowed for the study of various system parameters and road conditions under both line of sight and non-line of sight conditions, providing a reference value for vehicle safety navigation [6]. However, the above-mentioned technologies have limitations such as high computational complexity and high hardware resource requirements, which limit their widespread application in Agricultural Vehicle Navigation (AVN). To address the aforementioned issues, a Micro-inertial Navigation for Agricultural Vehicle Navigation (AVN-MN) method and a Point Cloud Registration (PCR) model combining Scale Invariant Feature Transformation Iterative Closest Point (SIFT-ICP) are proposed, namely the SIFT-ICP-MN model. The research innovation lies in three aspects: (1) The Scale Invariant Feature Transformation (SIFT) algorithm is introduced to improve the traditional Iterative Closest Point (ICP) algorithm, which has fallen into the local optima; (2) The SIFT-ICP model is used for PCR to obtain relative displacement and attitude change information of vehicles; (3) The calculation of position and velocity is introduced through a Micro-inertial Navigation (MIN) system, and precise navigation is achieved through data fusion technology.

The main contribution of the research is the proposal of an innovative AVN method. This method improves the traditional ICP algorithm by introducing the SIFT algorithm, improving the accuracy and robustness of PCR, and achieving accurate acquisition of vehicle relative displacement and attitude change information. At the same time, using MIN systems for position and velocity calculation, precise navigation is achieved through data fusion technology. The proposed method aims to improve the accuracy and stability of AVN, reduce its computational complexity and hardware resource requirements, and provide new ideas and methods for the development of AVN technology. This study consists of four sections. The first section is an overview of the present research status of the technologies used. The second section constructs a fusion of SIFT-ICP and AVN-MN. The third section conducts performance verification on the proposed method. The last section provides a summary and outlook for the entire paper. Table 1 is an abbreviation table of the article's terminology.

II. RELATED WORK

The point cloud ICP algorithm has achieved significant research results in the academic community, and many scholars have discussed it. To solve the problems of computing

TABLE 1. List of abbreviations and full names.

Abbreviation	Full name
ANP	Automatic Navigation and Positioning
SIFP	Scale Invariant Feature Transformation
PCR	Point Cloud Registration
SIFT-ICP	Scale Invariant Feature Transformation - Iterative Closest Point
MIN	Micro-inertial Navigation
AVN	Agricultural Vehicle Navigation
ICP	Iterative Closest Point
AFA	Adaptive Fireworks Algorithm
PCD	Point-cloud Data
SAC-IA	Sample Consensus Initial Alignment
ACF	Auto-correlation Function
TAA	Three-Axis Acceleration
TAV	three-axis angular velocity
EKF	Extended Kalman Filter
IMU	Inertial Measurement Unit
AVN-MN	Micro-inertial Navigation for Agricultural Vehicle Navigation

long and poor accuracy in 3D PCR, X Shi et al. proposed an improved k-dimensional tree ICP algorithm. This algorithm combined point cloud filtering and Adaptive Fireworks Algorithm (AFA) for coarse registration. Firstly, it filtered the Point-cloud Data (PCD) collected by the 3D laser scanner, and then used AFA for coarse registration. Through experimental verification of three physical models of statues, this method significantly improved computational speed and accuracy, and was stable and reliable [7]. F. A. Make et al. proposed a new algorithm for aligning two point clouds and accurately estimating the uncertainty of ICP transformation parameters. This method provided non parametric estimation of transformations, enabled modeling of complex multi-modal distributions, and enabled effective parallel computing on GPUs. Experiments using 3D Kinect data and sparse indoor/outdoor LiDAR data have shown that this method could effectively generate accurate pose uncertainty estimation [8]. I. Vizzo et al. utilized the point-to-point ICP algorithm with adaptive thresholds, robust kernels compensation methods, and point cloud sub-sampling strategies to estimate the pose of robots. This method relied entirely on 3D point-clouds obtained from various 3D LiDAR sensors and was suitable for a wide range of operating conditions. The system ran faster than the sensor frame rate and has been validated in real scenarios [9]. M. Brossard et al. proposed a new method to handle the uncertainty of 3D ICP and addressed error sources such as error convergence, under constraint situations, and sensor noise listed in Censi's work. The proposed method used an unscented transformation to reflect the correlation between initial and final uncertainties. This solution has been tested on real publicly available data from structured to unstructured environments, and the algorithm has predicted results consistent with actual uncertainty, with advantages over previous methods [10]. C. Lin et al. proposed an acceleration method to improve the ICP performance. This method utilized the two-dimensional features of azimuth images to

find corresponding point pairs, significantly improving registration speed. Simulation showed that this algorithm not only reduced the root mean square error of the initial attitude, but also reduced 75% of ICP iterations to a stable state. In addition, using 2D features on azimuth images as the initial ICP pose also improved robustness to larger perspective diversity [11].

Currently, AVN has attracted the attention of many scholars. X. Yin et al. developed an autonomous navigation controller that enables various agricultural vehicles to move autonomously. The hardware was used for program execution, data processing, and information exchanging with peripheral devices. The human-machine interface design allowed operators to finish basic settings, path planning, and navigation control. The versatility of the controller in targeting agricultural cars to travel along straight paths and turning at headlands were evaluated through field experiments. When completing linear navigation, the controller had good coping strategies [12]. P. Chhikara et al. proposed an autonomous navigation algorithm for goji berry orchards based on visual cues and fuzzy control, aiming to improve the harvesting efficiency of goji berries and reduce manual labor. This method utilized new weights (2.4B-0.9G-R) to convert color images into grayscale images to better recognize the trunk of goji berries, and used the minimum bounding rectangle to describe the outline of goji berries. This method could meet the automatic picking requirements of goji berry picking robots in real environments [13]. F. Rovira Más et al. designed a navigation system to guide robots in path planning in farmland. This method was based on local perception and utilized 3 complementary technologies: 3D vision, LiDAR, and ultrasound. Finally, the above three methods were integrated to form a complete intelligent behavior model for orchard operation robots based on the three methods. The integration of the above three technologies has laid a solid foundation for the intelligent operation of orchard operation robots [14]. M. Reger et al. delved into the use of LiDAR in harsh weather conditions in agricultural environments and conducted a series of field tests to evaluate in detail the performance of LiDAR in outdoor environments and its applicability in navigation. This study provided strong theoretical support and practical suggestions for using LiDAR as a navigation and collision avoidance technology in free navigation automatic feeding systems. This work provided new possibilities for achieving automatic navigation and obstacle avoidance of agricultural vehicles, and provided technical support for agricultural modernization and automation [15]. S. Gunturu et al. conceived and designed an innovative autonomous robot platform for agricultural robot navigation problems. This platform utilized spatial artificial intelligence technology to achieve effective collision avoidance during the free navigation of robots in crop rows. A spatial deep learning model was also trained to assist robots in autonomous navigation while avoiding crashing crops such as wheat. A detailed comparative analysis was conducted on

this method, revealing its effectiveness in model accuracy and inference speed [16].

In summary, ICP has achieved certain research results in various fields, and agricultural navigation models have also attracted the attention of many scholars. However, few studies have combined the two to explore the performance of agricultural vehicle ANP. Therefore, this study proposes the SIFT-ICP-MN fusion model aimed at overcoming the limitations of traditional navigation technology in agricultural environments and improving agricultural production efficiency.

III. CONSTRUCTION OF ANP AND OBSTACLE AVOIDANCE MODEL FOR AGRICULTURAL VEHICLES BASED ON ICP

This section mainly explores a PCR model combined with SIFT-ICP and AVN-MN method. This method aims to achieve precise, stable, and real-time navigation control of agricultural vehicles by integrating efficient PCR technology and MIN systems. This method uses the SIFT-ICP model for PCR to gain the relative displacement and attitude change of the vehicle, and calculates the position and speed through the MIN system. Finally, precise navigation is achieved through data fusion technology.

A. PCR MODEL BASED ON SIFT-ICP

Point cloud is an abundant point data obtained by measuring the outer surface of an object through sensors, which can display the spatial location and characteristics of the object. Sparse point clouds are point clouds with small data scales and large point intervals. A dense point cloud is a point cloud with numerous data and high point density. In Figure 1, point clouds can be segmented into 4 types based on the arrangement of points [17]. Figure 1 (a) shows a scattered point cloud with disordered structure and no significant relationship between points. Figure 1 (b) shows a grid point cloud, with data points arranged in an ordered queue, and each point corresponding to row and column coordinates. Figure 1 (c) shows the scanning line point cloud: multiple points form a scanning line, and multiple sets of scanning lines form a point cloud, with equal spacing between each line. Figure 1 (d) shows a polygonal point cloud: a nested planar polygonal point cloud is formed by connecting adjacent points with similar distances.

The ICP is an algorithm used for aligning 3D point clouds in two sets of spaces [18]. The basic idea of ICP is to iteratively find the rotation and translation matrix that minimizes the distance between the source and the target point clouds. The specific operation process includes selecting corresponding points, calculating transformation matrices, updating the position of the source point cloud, and iterating repeatedly until the set termination conditions are met. The main function of ICP is PCD registration, which can be used to obtain accurate poses of objects or fuse PCD collected from various aspects and times [19]. Therefore, its application scenarios are very extensive, such as in robot navigation, object

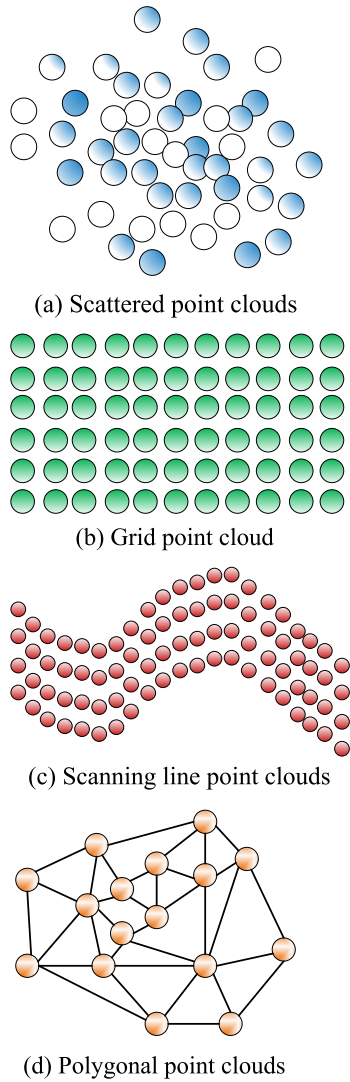


FIGURE 1. Classification of PCD.

recognition, medical image processing, terrain surveying and other fields. Figure 2 shows the registration process of ICP.

The ICP algorithm achieves precise registration of point clouds by searching for the nearest neighbor relationship between two point sets and calculating rotation and translation parameters, iterating continuously until the termination conditions are met [20]. Assuming the target set is S and the set of points to be registered is T . For each point in the T to be registered, to find its nearest point in the target point set S and form a corresponding point pair sequence, as shown in equation (1).

$$Y = F(T, X) \tag{1}$$

In equation (1), Y represents the set of all nearest points. F represents the mapping relationship between each point and its nearest neighbor. X represents the nearest point corresponding to T . The rigid body transformation matrix based on the relationship between the corresponding point pairs is

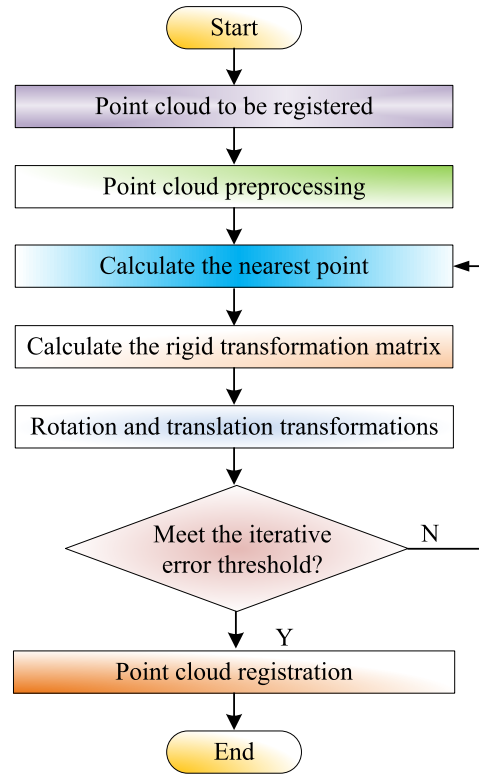


FIGURE 2. ICP registration process.

calculated, and this transformation matrix is used to transform the set of points to be registered into a new coordinate point set, as shown in equation (2).

$$T' = T * R_{3*3} + T_{1*3} \tag{2}$$

In equation (2), R_{3*3} is the rotation matrix. T_{1*3} means the translation matrix. T' represents a new set of coordinate points. The distance calculation formula between the target and the new alignment point sets is equation (3).

$$RMS(S, T') = \frac{1}{q} \sum_{i=1}^q (|T'_i - S_j|)^2 < \sigma, \quad (1 \leq j \leq p) \tag{3}$$

In equation (3), p and q are the quantity of points of S and T . T'_i represents each point in the set of alignment points to be matched. S_j represents the closest point of point T'_i in the target point set. σ represents the preset minimum distance threshold. The traditional ICP algorithm is widely used in PCR in various industries. Compared to other algorithms, its registration accuracy is high and the input data requirements are low. Accurate registration can be achieved with only 3D coordinates [21], [22]. However, ICP also has some shortcomings. Firstly, ICP has a strong dependence on the initial position. If the initial positions of two point clouds differ too far, it may lead to the algorithm converging to a local optimal solution rather than a global optimal solution. Secondly, the convergence speed of ICP algorithm is relatively slow, especially when dealing with large-scale PCD. In addition, the

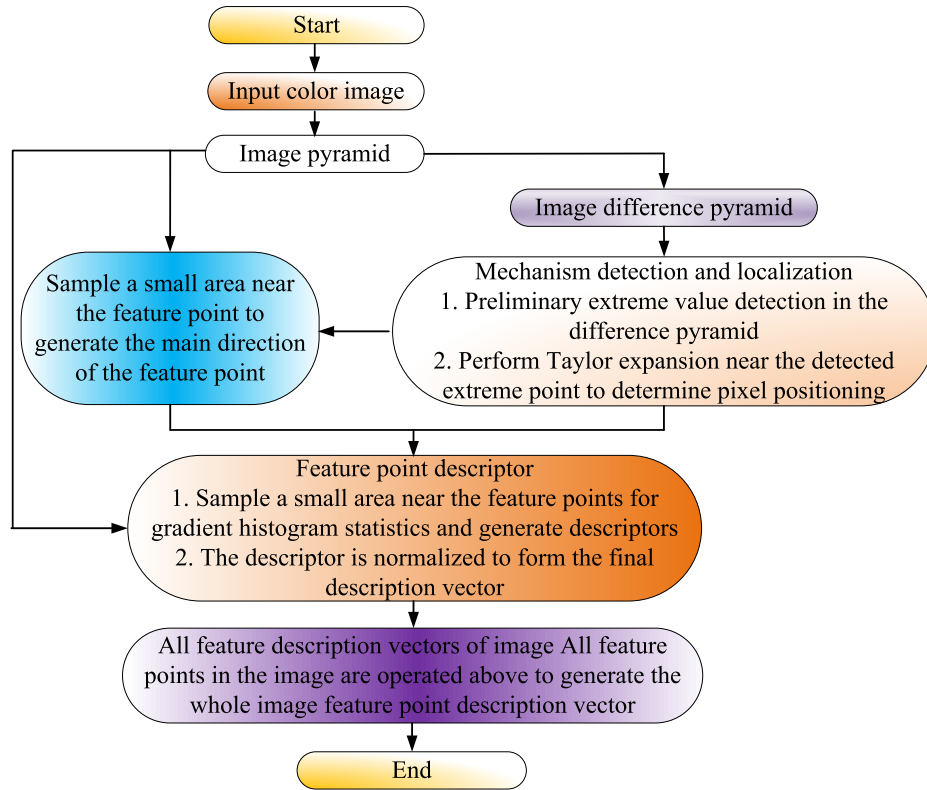


FIGURE 3. Implementation process of SIFT.

ICP algorithm requires users to preset some parameters, such as iteration times, error thresholds, etc. Improper parameter selection may affect the effectiveness of the algorithm. Therefore, the improvement and optimization of ICP algorithm is still an important research topic at present.

The SIFT algorithm is a feature matching algorithm that transforms an image into a set of local feature vectors with multiple in-variances to find matching feature point pairs [23], [24]. The advantages of SIFT algorithm include: it has good local feature extraction ability for various changes. It can achieve fast and accurate matching in large amounts of data, and extract rich feature vectors even when objects are sparse. It has good scalability and can be used in combination with other feature vectors. The SIFT algorithm consists of several steps: establishing a differential scale space and detecting feature points, describing the pixel information of feature points and their surrounding influences, producing feature point descriptors, and comparing feature point descriptors for feature point matching. The implementation process of SIFT is Figure 3.

In the fields of image processing and 3D PCR, SIFT and ICP algorithms respectively play important roles with their unique advantages. SIFT excels in feature point detection and relationship extraction, achieving preliminary registration of point clouds. ICP completes the fine adjustment of the registration process with its precise optimal matching ability. This study innovatively combines the two and proposes the

SIFT-ICP PCR model. This model first uses SIFT to extract key feature points of the point cloud to be registered and the target, and then calculates the FPFH features of these points. Based on these features, the Sample Consensus Initial Alignment (SAC-IA) algorithm is used to obtain the transformation matrix and achieve preliminary registration. Finally, the preliminary registration results are finely adjusted using the ICP algorithm, achieving efficient and accurate PCR. The scale space generated by SIFT is equation (4).

$$L(x, y, \delta) = G(x, y, \delta) \otimes I(x, y) \quad (4)$$

In equation (4), δ represents the scale space factor. (x, y) represents the pixel coordinates of the image. $I(x, y)$ is the original image. $G(x, y, \delta)$ represents a variable scale Gaussian function. To detect extreme points in the scale space and construct a Gaussian difference function, as shown in equation (5).

$$\begin{aligned} D(x, y, \delta) &= [G(x, y, k\delta) - G(x, y, \delta)] \otimes I(x, y) \\ &= L(x, y, k\delta) - L(x, y, \delta) \end{aligned} \quad (5)$$

In equation (5), δ represents the scaling factor of two adjacent Gaussian scale spaces. The calculation formula for FPFH is equation (6).

$$F(M_q) = S(M_q) + \frac{1}{k} \sum_{i=1}^k \omega_i \cdot S(M_q) \quad (6)$$

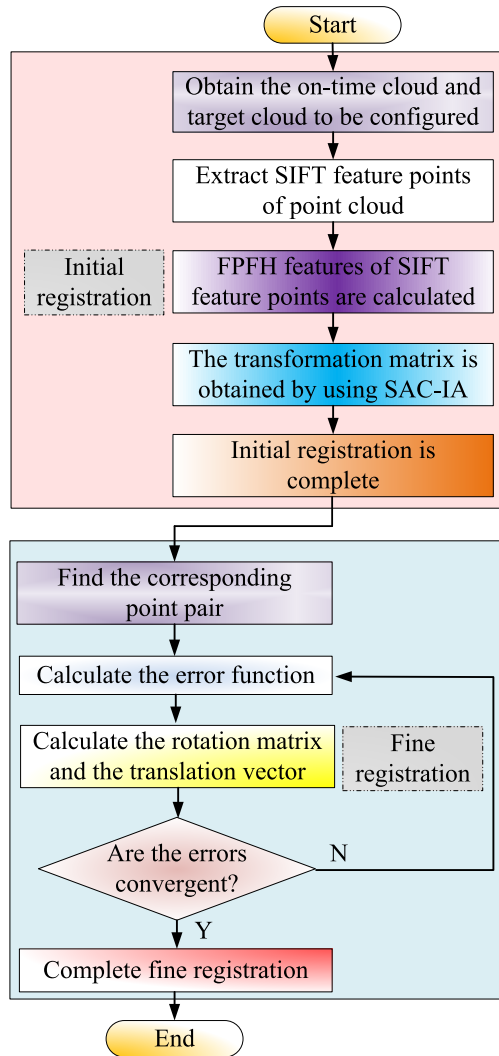


FIGURE 4. Running flow of point cloud registration in SIFT-ICP model.

In equation (6), M_q represents the point to be calculated. $S(M_q)$ represents a simplified point feature histogram. ω_i is the weighted value of the i -th neighborhood point. $\frac{1}{\omega_i}$ represents the distance value between the point to be calculated and its i -th neighboring point. SAC-IA solves the transformation relationship as shown in equation (7).

$$H(l_i) = \begin{cases} \frac{1}{2}l_i^2, & \|l_i\| < m_l \\ \frac{1}{2}m_l(2\|l_i\| - m_l), & \|l_i\| \geq m_l \end{cases} \quad (7)$$

In equation (7), m_l represents a preset value. l_i is the distance difference between the corresponding points in Group i after transformation. Therefore, the operational process of the SIFT-ICP model constructed in this study is Figure 4.

B. PCR MODEL AND AVN-MN COMBINING SIFT-ICP

AVN and obstacle avoidance technology are important components of agricultural automation, which are related to the

efficiency and safety of agricultural production. However, this field faces many challenges [25]. On the one hand, the agricultural condition is complex and changeable, and changes in weather, soil, and crop growth status can all have an impact on vehicle navigation and obstacle avoidance. On the other hand, agricultural vehicles often operate without human monitoring, requiring navigation and obstacle avoidance systems to have a high degree of autonomy and stability. In addition, to improve agricultural production efficiency, agricultural vehicles need to be able to perform precise path planning and motion control, which puts higher requirements on navigation and obstacle avoidance technology. At present, researchers are working hard to solve these problems and promote the development of AVN and obstacle avoidance technology through technological innovation and system optimization.

The MIN system uses micro-sensors to measure acceleration and angular velocity, and calculates position and velocity through integration. The PCR model provides precise positional information, but may encounter issues in dynamic environments or visual occlusion. The MIN system can operate in any environment, but the accumulation of measurement errors will reduce accuracy [26]. The combination of the two can use another system to provide auxiliary information and improve navigation performance when a problem occurs in one system. The fusion of visual and inertial information using PCR model and MIN system navigation technology can improve navigation accuracy and robustness, making it suitable for robots, autonomous vehicles, and drones [27]. The MIN system mainly relies on Newton's second law to calculate position and velocity. The accelerometer mainly consists of three parts: mass block, spring, and damping [28], [29]. The resultant force of an object is equal to the product of its mass and acceleration. By measuring the combined force of the mass blocks inside the accelerometer, the acceleration of an object can be obtained. When there is no external force, the mass block is in a free state, and its position serves as the origin. When the base accelerates, the spring deforms due to inertial forces, pushing the direction of the force back out. According to Newton's second law, equation (8) can be obtained.

$$m(\ddot{x} + a) = -D\dot{x} - cx - mg \quad (8)$$

In equation (8), m , \ddot{x} , and \dot{x} are the mass, acceleration and speed of the mass block. a represents the acceleration of the mass block's motion. c and x are the stiffness coefficient and deformation of the spring. D is the damping coefficient. g represents gravitational acceleration. f is defined as the external force acting on a unit mass, and there is equation (9).

$$f = F_t/m \quad (9)$$

In equation (9), F_t represents the spring force. m represents the mass of a mass block. By combining equations (8) and (9), equation (10) can be obtained.

$$f = a + g \quad (10)$$

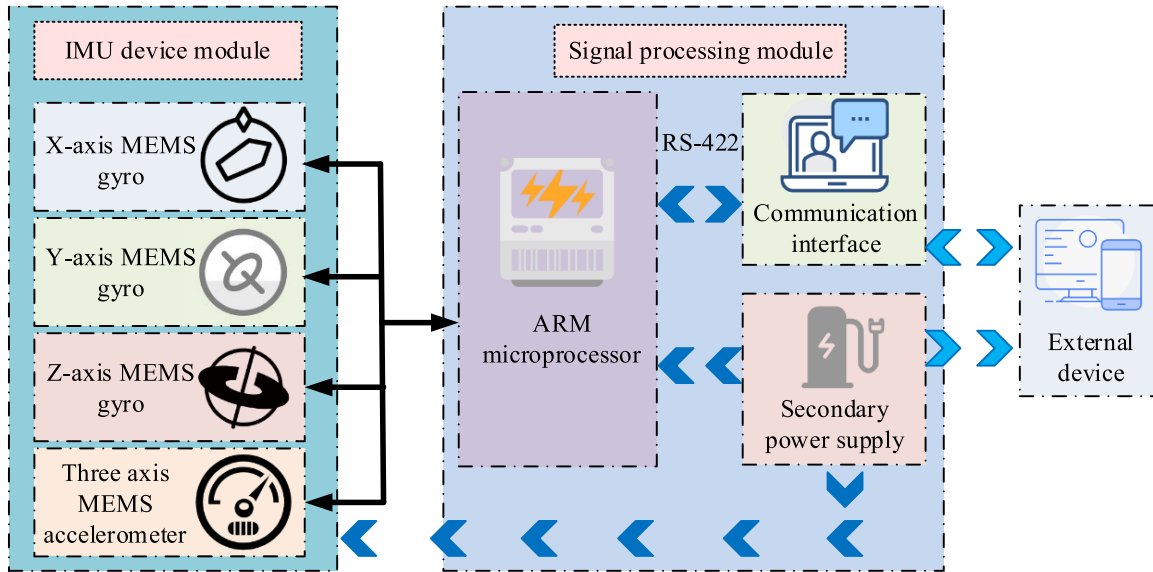


FIGURE 5. Micro-inertial system measurement unit system diagram.

Equation (10) shows that due to the limitations of the accelerometer in distinguishing between inertial acceleration and gravitational acceleration, there may be some errors in its resolution results. To obtain more accurate acceleration, the gravitational acceleration g needs to be subtracted from f to obtain a . The Inertial Measurement Unit (IMU), as the core of the inertial navigation system, integrates sensors such as accelerometers and gyroscopes, and has the advantages of autonomous navigation and no environmental interference. Its system framework is shown in Figure 5.

This study utilizes a commercial grade attitude reference system that integrates gyroscopes, accelerometers, magnetometers, thermometers, and barometers. All sensor measurements are temperature compensated and unified into one coordinate system. The system can output the original measurement values of all sensors, as well as the attitude and covariance relative to the local horizontal coordinate system [30], [31]. The error of inertial devices greatly affect the inertial navigation accuracy, so it is necessary to compensate for the error sources and sizes of inertial devices. When the accelerometer is placed in a stationary state, regardless of the attitude, the sum of squared true values of the measured acceleration satisfies equation (11).

$$f_x^2 + f_y^2 + f_z^2 = g^2 \tag{11}$$

In equation (11), f_x^2, f_y^2, f_z^2 represents the square of the Three-Axis Acceleration (TAA) values of x, y, z . g is the local gravitational acceleration constant. The three-axis measurement value calculation formula of the accelerometer is

equation (12).

$$\begin{cases} \bar{f}_x = a_1 f_x + a_2 \\ \bar{f}_y = a_3 f_y + a_4 \\ \bar{f}_z = a_5 f_z + a_6 \end{cases} \tag{12}$$

In equation (12), a_1, a_3, a_5 are the scale factor parameters. a_2, a_4, a_6 are the fixed errors of the accelerometer. In a stationary state, the IMU is placed in different postures for a period of time, and the equation (12) corresponding to the average acceleration value during each stationary time period is introduced into equation (11) to obtain a set of equations. Then, the least squares fitting is used to determine the $a_1 \sim a_6$ parameters. Regarding the fixed error calibration of gyroscopes, it is generally possible to obtain the average value of the gyroscope over a short period of time by using a stationary instrument during initial power on [32], [33]. The selection of a random error model depends on the instrument's operating time, condition, and experimental environment. Short-term operation can consider fixed errors, while long-term operation requires consideration of random errors. For the random error of inertial devices, this study mainly uses auto-correlation method. A random process and its correlation function are called Auto-correlation Functions (ACF), and their expression is equation (13).

$$R(t_1, t_2) = E(x(t_1)x(t_2)) \tag{13}$$

In equation (13), t_1, t_2 are any sampling time. R represents the correlation coefficient. E represents mathematical expectation. The unit of the ACF is the square of the unit of the random process signal. The ACF of a random process represents the correlation degree between signals at various time points [34]. When the probability density function of

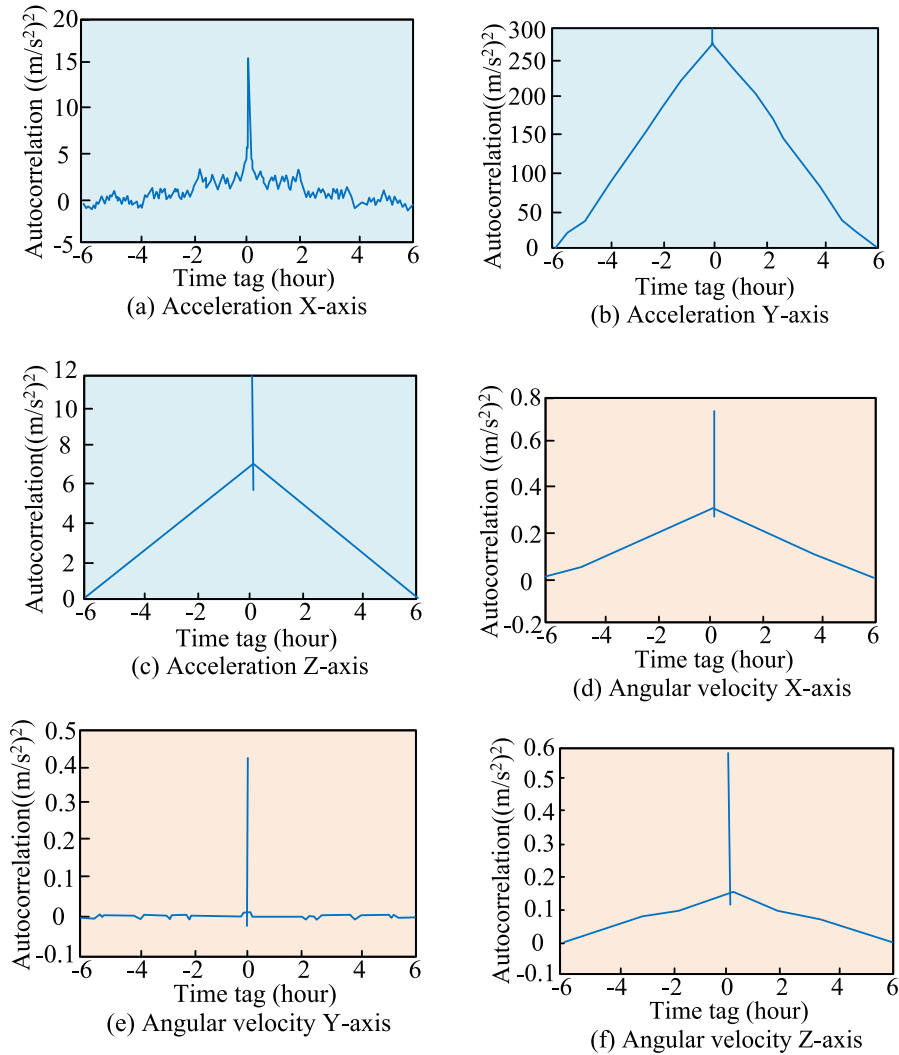


FIGURE 6. ACF image of IMU.

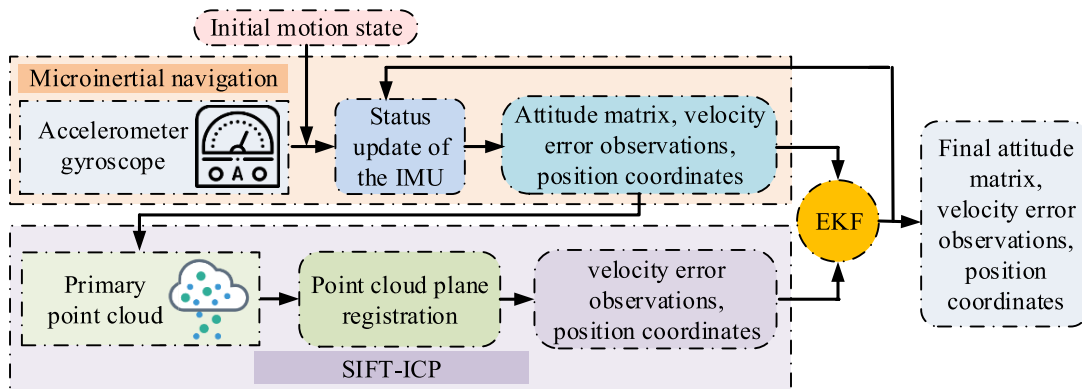


FIGURE 7. Navigation model of agricultural vehicle based on SIFT-ICP-MN.

a random process does not change over time, it can be said that the random process is stationary. The ACF of this stationary random function is only related to $\tau = t_1 - t_2$, and

equation (13) can be transformed into equation (14).

$$R(\tau) = E(x(t)x(t + \tau)) \quad (14)$$

The ACF image of the IMU used in this study is shown in Figure 6. Figure 6(a) - 6(f) represent the time correlation analysis of different signals in the IMU, where Figure 6(a) - 6(c) represent the autocorrelation of TAA, and Figure 6(d) - 6(f) represent the autocorrelation of Three-axis Angular Velocity (TAV). Among them, the ACF of TAA is used to analyze the correlation of TAA signals in time series. The ACF of TAV is used to study the correlation of TAV signals in time series. The six sets of ACF images shown in the figure all exhibit similar trends, similar to a normal distribution. This trend can effectively depict the gradually evolving errors in inertial navigation systems, which helps to gain a deeper understanding of the dynamic characteristics of navigation errors [35]. By calculating the auto-correlation values of the signal at different times, the temporal stability, periodicity, and other characteristics of the signal can be obtained, which is of great significance for understanding and predicting the behavior of TAA.

After obtaining the accurate initial attitude, velocity, and position, the carrier position and attitude can be calculated using inertial navigation algorithms using the measured values of inertial devices with errors and Newton's laws. However, the accumulation of errors is inevitable, so it is necessary to simultaneously model and estimate the changes in the system error state. Based on Newton's laws of motion, equation (15) presents the inertial navigation motion, taking into account the Earth's rotation and the movement of the carrier/Earth coordinate system.

$$\dot{X}(t) = F(t)X(t) + Gu \quad (15)$$

In equation (15), $F(t)$ represents the system state matrix. G represents the noise coefficient matrix. u represents the system noise vector.

PCR can obtain the relative displacement and attitude changes between adjacent frames. By integrating Extended Kalman Filter (EKF) with IMU pose estimation for data fusion, the advantages and disadvantages of both can be integrated to achieve more stable and efficient navigation and obstacle avoidance. This study uses EKF, combined with LiDAR and IMU to achieve navigation obstacle avoidance. Firstly, the initial attitude of the IMU is obtained through initial fine calibration. In the filtering body, the carrier motion and system error status are updated every time the IMU measurement value is updated. When new LiDAR PCD is generated, it is restored to the horizontal coordinate system through IMU attitude, and then the point cloud displacement and velocity are obtained through plane registration, which are used as filtering observations to update the system error status and agricultural vehicle status. The fusion model SIFT-ICP-MN is shown in Figure 7. In Figure 7, the SIFT-ICP-MN model first uses SIFT-ICP to accurately register PCD. This model can capture and analyze the relative displacement and attitude change information of vehicles, thereby providing key data for navigation. Subsequently, the MIN system performs real-time calculations of position and velocity based on this information. Finally, through advanced data fusion

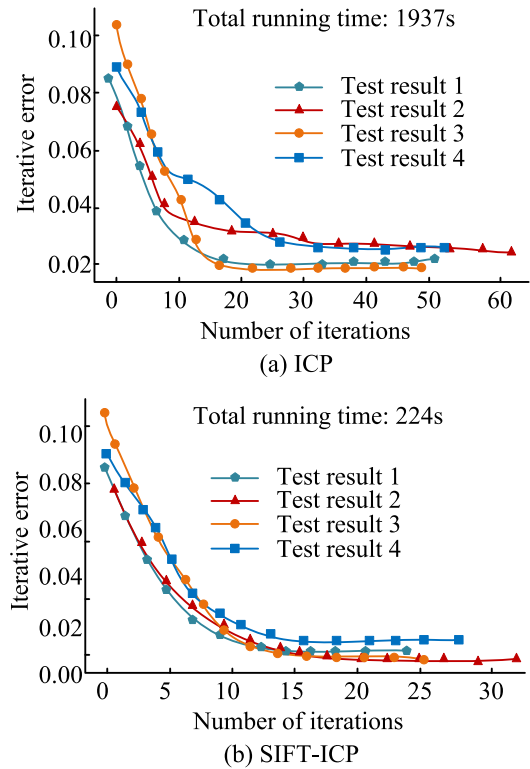


FIGURE 8. Iterative relationship between traditional ICP and SIFT-ICP.

technology, the two information are effectively combined to achieve navigation accuracy and stability.

IV. PERFORMANCE VERIFICATION OF ANP AND OBSTACLE AVOIDANCE MODEL FOR AGRICULTURAL VEHICLES BASED ON ICP

This study mainly focuses on the performance verification of ANP and obstacle avoidance models for agricultural vehicles, especially the navigation model based on ICP. Firstly, performance analysis of the SIFT-ICP-based PCR model is conducted by collecting and processing PCD obtained from LiDAR scanning. Then, through a series of experiments, the performance of the SIFT-ICP-MN model is thoroughly tested and analyzed.

A. PERFORMANCE ANALYSIS OF PCR MODEL BASED ON SIFT-ICP

To verify the algorithm's reliability and stability, as well as the practicality of the PCR program, a vehicle mounted laser point cloud dataset from a certain orchard scene is selected as experimental data in this study, ensuring the practicality and reliability of the experiment. The experiment uses a self-developed PCR program, combined with SSW vehicle system supporting software and open-source software, to display PCD and evaluate registration results. The experimental equipment is a laptop with the Win10 operating system. The cloud server is mainly responsible

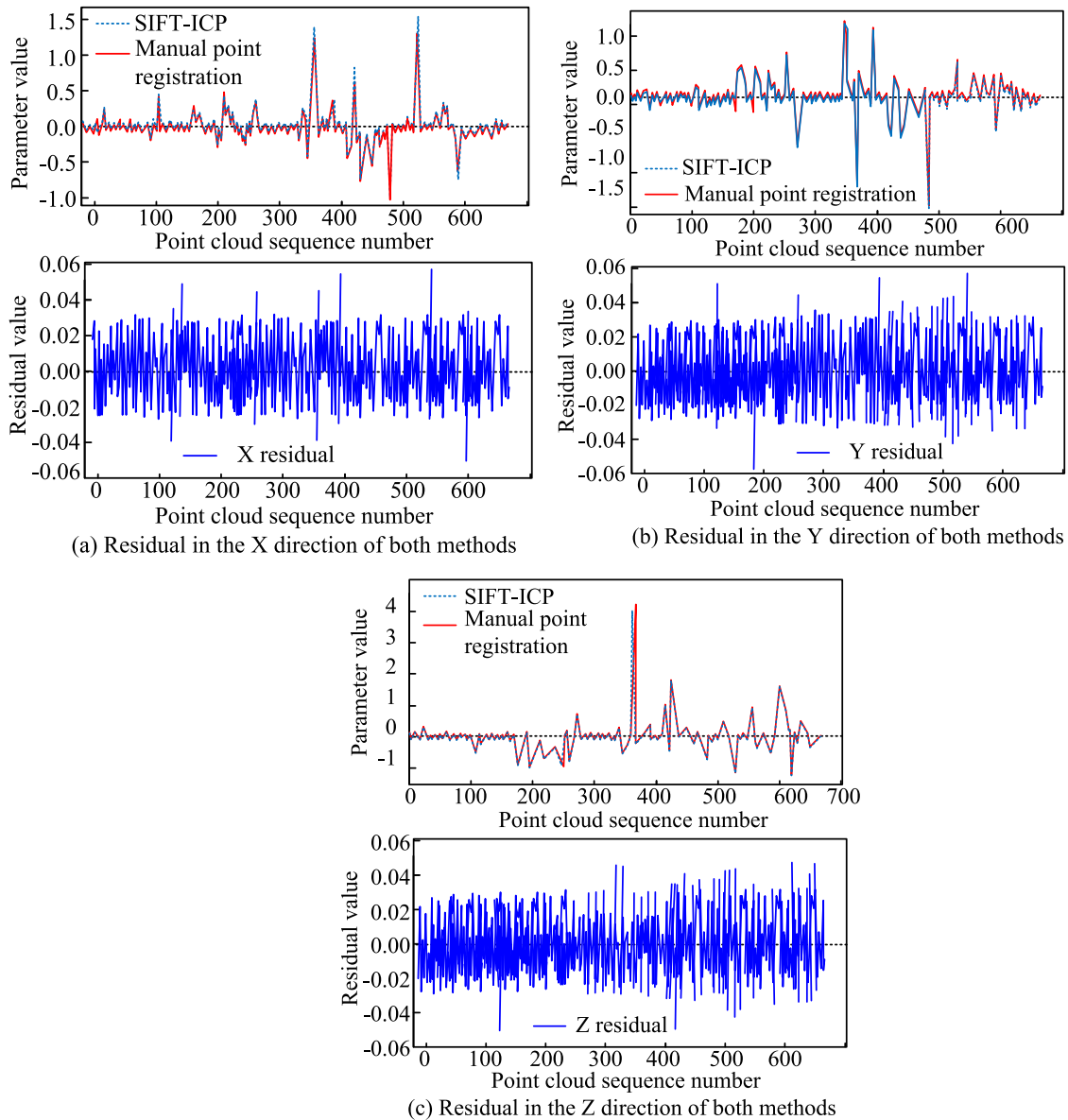


FIGURE 9. PCR results of SIFT-ICP algorithm.

for PCR work. In the experiment, there are approximately 500,000 point clouds to be registered in each group, and a thread pool is used to perform asynchronous parallel processing of multiple files. The algorithm parameters are set after comprehensive consideration of registration accuracy and efficiency. Table 2 is the settings of the main recommended parameters.

This study uses an iterative relationship graph to evaluate the convergence speed of the ICP on the same PCD, providing a reference for analyzing the registration schemes of traditional ICP and SIFT-ICP algorithms. This study divides a certain section of the orchard into four sections of test data. The iterative relationship between traditional ICP and SIFT-ICP is shown in Figure 8. Compared to SIFT-ICP,

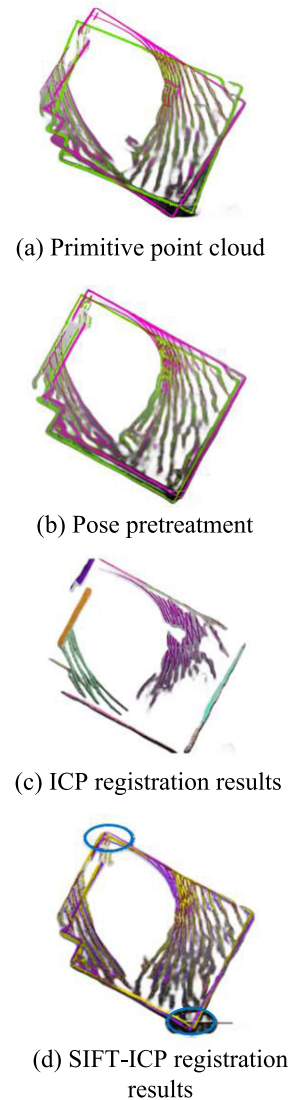
traditional ICP requires more iterations. In the first 30 iterations, both deviations are inversely proportional to the number of iterations, but SIFT-ICP shows a significant and rapid reduction in error in the first 10 iterations, demonstrating its high efficiency and error convergence speed. In terms of accuracy, traditional ICP is hard to cater for the accuracy and efficiency needs of in vehicle laser PCR, and there is a risk of significant errors that cannot converge. The traditional ICP registration time is about 400s~500s, and SIFT-ICP is about 60s, with the latter increasing efficiency by 8.6 times. Under the same parameter conditions, the SIFT-ICP algorithm can significantly shorten the running time and improve efficiency by more than 10 times, demonstrating its advantages in registration efficiency.

TABLE 2. Experimental parameter settings.

Parameter	Numerical value
Number of point cloud segments	4
Overlap area	$\geq 140\text{m}^2$
Minimum number of point clouds	40
Neighborhood radius	0.5m
Voxel grid size	0.05m
Gradient threshold	0–0.14
Maximum iterations	500
Fixed range threshold	0.45
Upper limit of dynamic range factor	0.6m
Lower limit of dynamic range factor	0.3m
Iterative decreasing unit	0.02m
Cumulative times threshold	35
Number of parallel threads (adjustable)	12
Error threshold	$2 \times 10^{-2}\text{m}$

To accurately evaluate the registration accuracy of the SIFT-ICP, this study compares the results of manually selected points and measures corresponding positions, and calculates the parameter residuals between the two from the x, y, and z directions. This comparison method can use the results of actual operations as a standard to provide a more intuitive and accurate evaluation of the accuracy of the algorithm. Figure 9 shows the PCR results of the SIFT-ICP algorithm. The error situation between vehicle mounted laser PCD is quite complex and has significant variability. For example, the maximum deviation in the elevation direction can reach more than 4m. Despite facing such complex PCD and significant biases, the SIFT-ICP still demonstrates high registration accuracy in experiments. Except for a few locations with slightly larger point deviations, the overall error value remains stable within the range of -0.03m to 0.03m . This result fully demonstrates the stability and reliability of the SIFT-ICP in processing complex PCD matching, demonstrating its excellent performance in practical applications.

This study takes orchard PCD as an example to conduct planar registration experiments. Two sets of point clouds separated by 40 frames are selected as experimental objects. First, the pose between the two is initialized, and then the corresponding plane relationship for registration is extracted to obtain the rotation matrix and translation parameters. Figure 10 shows a comparison of PCR results between two algorithms. Figures 10 (a) and 10 (b) correspond to the results of the SIFT-ICP algorithm, showing good registration accuracy, tight alignment between point clouds, and accurate matching of planar relationships. Figures 10 (c) and 10 (d) show the results of the traditional ICP algorithm, which presents a situation of low registration accuracy, with significant misalignment, especially in the areas highlighted by circular annotations in Figure 10 (d), which may indicate significant registration errors. This indicates that the algorithm is susceptible to the influence of local optimal solutions when dealing with sparse point clouds, leading to inaccurate registration. In contrast, SIFT-ICP is based on planar features, and as long as there are sufficient planar features in the scene, even if the point cloud is sparse, accurate rotation and

**FIGURE 10. Comparison of cloud registration results.**

translation parameters can be obtained, which is superior to the ICP algorithm.

B. PERFORMANCE ANALYSIS OF THE FUSION MODEL SIFT-ICP-MN

After obtaining the plane registration results of all point clouds, the G2O graph optimization library is used to perform nonlinear optimization on all plane registration results, obtaining a set of approximate real trajectory attitude information. By utilizing this set of trajectory postures, the mutual position and attitude relationships of all point clouds are restored, and a dense point cloud model of the entire orchard is obtained. The experimental results of the combined navigation strategy are analyzed from two aspects: the accuracy of attitude estimation and displacement estimation.

Before analyzing the trajectory accuracy of SIFT-ICP-MN integrated navigation, it is essential to understand the

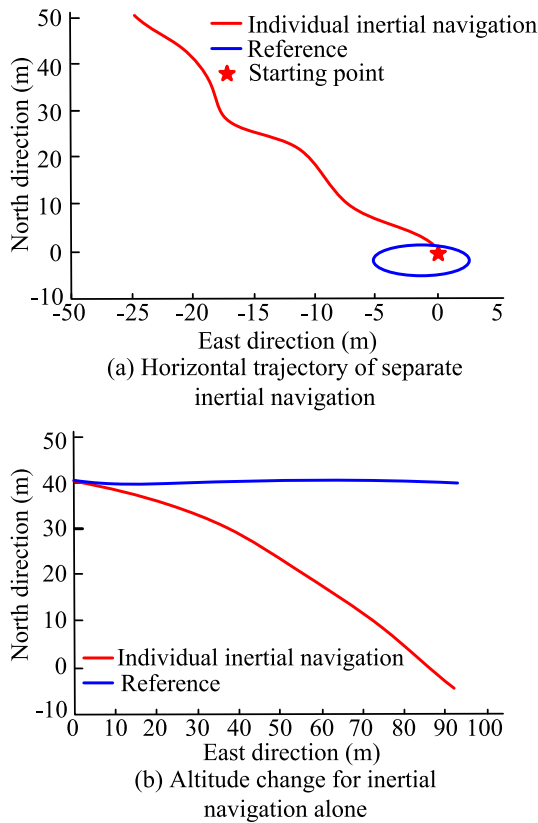


FIGURE 11. Trajectory drift of single inertial navigation.

trajectory drift situation of individual inertial navigation. In Figure 11, using inertial navigation alone will result in a large amount of drift in the short term, and in this case, it cannot meet the needs of orchard navigation. The emergence of this drift causes the accuracy of inertial navigation systems to rapidly decline over time when external information cannot be obtained. Therefore, it is necessary to use SIFT-ICP plane registration to constrain the error drift. Through this approach, the cumulative error of the system can be effectively corrected, thereby improving the accuracy of the overall navigation system.

Figure 12 compares the SIFT-ICP-MN calculated pose with the popular GPS LiDAR and reference pose. The results show that the pitch angle and roll angle errors of SIFT-ICP-MN are smaller compared to the attitude angle errors obtained by GPS-LiDAR plane registration. The heading angle error is similar to GPS LiDAR, but the cumulative error of GPS LiDAR increases over time. This is because the gyroscope accuracy of SIFT-ICP-MN is high, its attitude accuracy is not easily affected by plane extraction noise, and the gyroscope output always remains uninterrupted, while plane registration may cause mismatches and interruptions. Therefore, the method of using GPS-LiDAR attitude correction system attitude error is not advisable in EKF design.

Figure 13 shows the trajectory and error comparison of two methods in the horizontal direction. In Figure 13 (a),

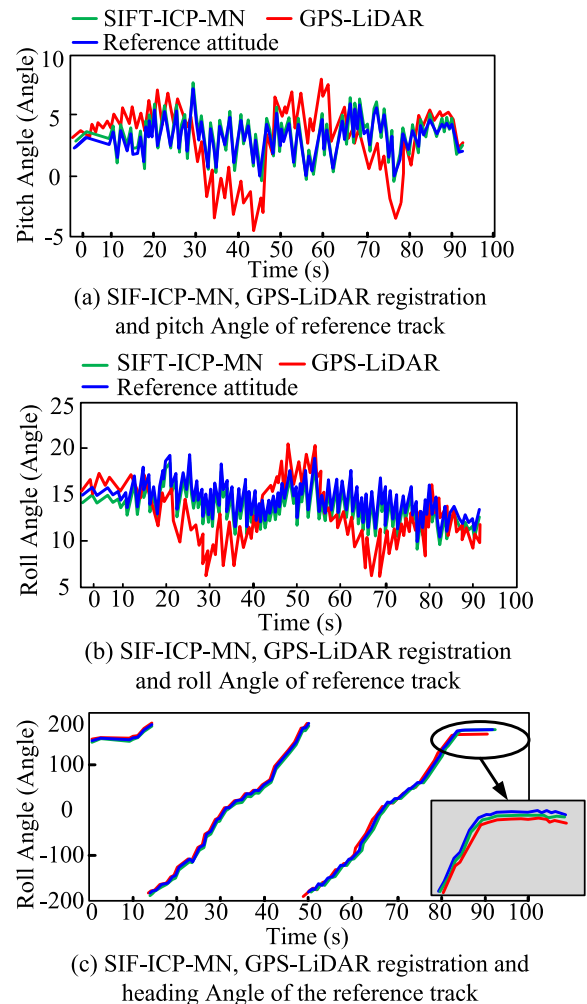


FIGURE 12. Comparison results of SIFT-ICP-MN, GPS-LiDAR plane registration and attitude Angle of reference trajectory.

the trajectory performance of SIFT-ICP-MN in the horizontal direction is better, and although its error increases over time, it is faster than the rapid drift of inertial navigation alone. SIFT-ICP-MN effectively suppresses error drift, with a horizontal error of 0.3m at the filtering trajectory endpoint. In Figure 13 (b), even if there is significant drift in the SIFT-ICP-MN point cloud plane registration, the filtered error remains within a small range. This indicates that the integrated navigation system has a certain degree of independence in the plane registration error of laser point clouds, and even if there are problems with plane registration, it can maintain trajectory accuracy for a period of time.

This study conducts a series of experiments based on a dataset in a daytime vehicle environment to verify the effectiveness and accuracy of SIFT-ICP-MN, and the results are showed in Figure 14. In the experiment, SIFT-ICP-MN achieves a distance accuracy of 84.88%, indicating that it can predict or calculate the actual distance with nearly 85% accuracy. Meanwhile, SIFT-ICP-MN achieves 97.63% accuracy

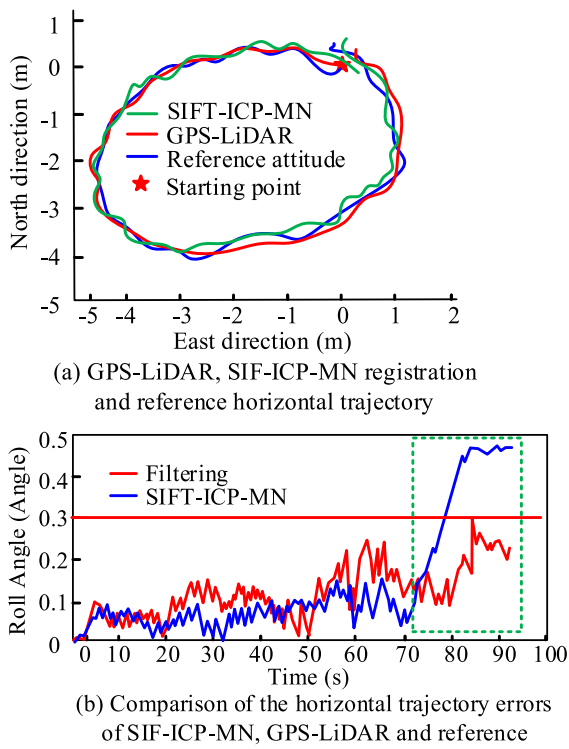


FIGURE 13. Comparison of horizontal trajectories and errors of the two methods.

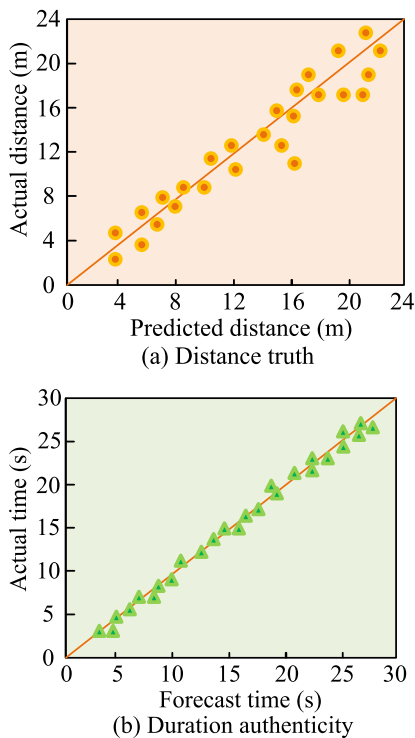


FIGURE 14. Distance truth and duration truth of SIFT-ICP-MN.

in terms of duration. This indicates that SIFT-ICP-MN can predict or calculate the actual time length with an accuracy

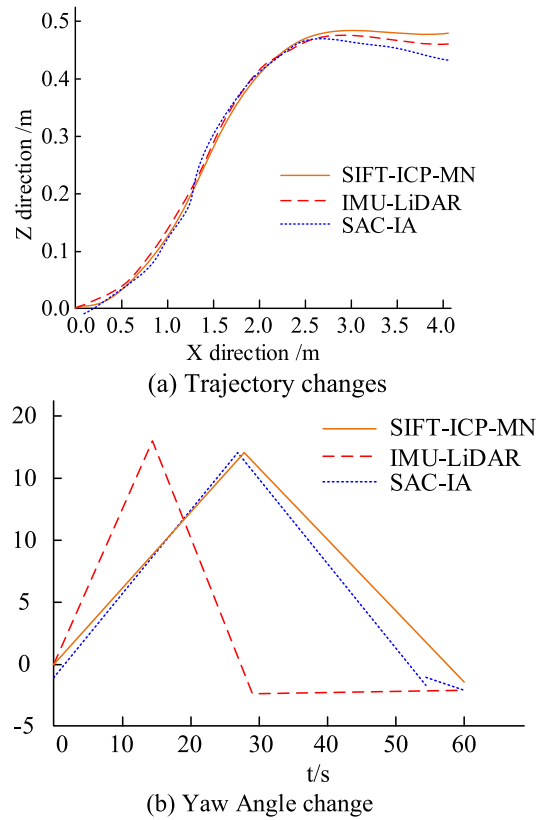


FIGURE 15. Changes of moving tracks of three models at different reference speeds.

of nearly 98%. These two data validate the effectiveness and SIFT-ICP-MN accuracy.

To highlight the superiority of SIFT-ICP-MN model, the study chooses to compare and verify it with the existing obstacle avoidance technology for agricultural vehicles, namely, the sampling consistency initial registration method (SAC-A) and the combined navigation method of IMU-LiDAR. Figure 15 shows the moving orbit of the three models at different reference velocities. In Figure 15 (a), the trajectories of the three models almost overlap with the reference trajectory, demonstrating good tracking ability. In Figure 15 (b), all models also closely follow the reference trajectory, but the trajectory of the SIFT-ICP-MN model matches the reference trajectory more closely, indicating that it exhibits more accurate performance in trajectory tracking and yaw angle adjustment. Compared with the other two methods (SAC-IA and IMU LiDAR combined navigation), its advantages are particularly obvious. At different reference speeds, the three models can track the reference trajectory well, and the error is within the predetermined range. SIFT-ICP-MN tracks the orbit and yaw angle well compared to SAC-IA and IMU-LiDAR.

V. CONCLUSION

At present, the level of agricultural mechanization and intelligence is constantly improving. The precise positioning and

safety obstacle avoidance technology of agricultural vehicles has become a key link in agricultural production. This study proposed a multi-modal integrated navigation strategy that integrated SIFT-ICP and MIN, and conducted simulation experiments to analyze it. The PCR model experiment based on SIFT-ICP demonstrated that SIFT-ICP exhibited fewer iterations, a faster error convergence speed, and a reduced risk of error non-convergence in comparison to traditional ICP. The registration time of SIFT-ICP was about 60 seconds, which was 8.6 times more efficient than traditional ICP (400s~500s). The error value of the SIFT-ICP algorithm was generally stable within the range of -0.03m to 0.03m in the overall situation. Even if the point cloud was sparse, SIFT-ICP could obtain accurate rotation and translation parameters, which is superior to the ICP algorithm. The comparison between SIFT-ICP-MN attitude estimation and GPS-LiDAR attitude showed that the pitch and roll angle errors of SIFT-ICP-MN were smaller compared to the attitude angle errors obtained by GPS-LiDAR plane registration. The heading angle error was similar to GPS-LiDAR, but the cumulative error of GPS-LiDAR increased over time. SIFT-ICP-MN could effectively suppress error drift, with a horizontal error of 0.3m at the filtering trajectory endpoint. The experimental distance accuracy based on the vehicle mounted daytime environment dataset was 84.88%, and the duration accuracy was 97.63%. SIFT-ICP-MN can effectively navigate and avoid obstacles, which is really meaningful for modern agricultural production. The limitation of this study is that inertial navigation is susceptible to the influence of gravitational acceleration, which poses challenges in navigation in complex environments. Further research is needed on how to combine other constraints to control the vertical error drift of IMU.

REFERENCES

- [1] L. Li, M. Yang, L. Weng, and C. Wang, "Robust localization for intelligent vehicles based on pole-like features using the point cloud," *IEEE Trans. Autom. Sci. Eng.*, vol. 19, no. 2, pp. 1095–1108, Apr. 2022, doi: [10.1109/TASE.2020.3048333](https://doi.org/10.1109/TASE.2020.3048333).
- [2] H. Yang, J. Shi, and L. Carlone, "TEASER: Fast and certifiable point cloud registration," *IEEE Trans. Robot.*, vol. 37, no. 2, pp. 314–333, Apr. 2021, doi: [10.1109/TRO.2020.3033695](https://doi.org/10.1109/TRO.2020.3033695).
- [3] S. Quan and J. Yang, "Compatibility-guided sampling consensus for 3-D point cloud registration," *IEEE Trans. Geosci. Remote Sens.*, vol. 58, no. 10, pp. 7380–7392, Oct. 2020, doi: [10.1109/TGRS.2020.2982221](https://doi.org/10.1109/TGRS.2020.2982221).
- [4] Y. Zhou, Y. Yang, B. Zhang, X. Wen, X. Yue, and L. Chen, "Autonomous detection of crop rows based on adaptive multi-ROI in maize fields," *Int. J. Agricult. Biol. Eng.*, vol. 14, no. 3, pp. 217–225, Apr. 2021, doi: [10.25165/j.ijabe.20211404.6315](https://doi.org/10.25165/j.ijabe.20211404.6315).
- [5] F. Aghaei, H. B. Eldeeb, L. Bariah, S. Muhaidat, and M. Uysal, "Comparative characterization of indoor VLC and MMW communications via ray tracing simulations," *IEEE Access*, vol. 11, pp. 90345–90357, 2023, doi: [10.1109/ACCESS.2023.3307186](https://doi.org/10.1109/ACCESS.2023.3307186).
- [6] F. Aghaei, H. B. Eldeeb, and M. Uysal, "A comparative evaluation of propagation characteristics of vehicular VLC and MMW channels," *IEEE Trans. Veh. Technol.*, vol. 73, no. 1, pp. 4–13, Jan. 2024, doi: [10.1109/TVT.2023.3302991](https://doi.org/10.1109/TVT.2023.3302991).
- [7] X. Zhan, Y. Cai, H. Li, Y. Li, and P. He, "A point cloud registration algorithm based on normal vector and particle swarm optimization," *Meas. Control*, vol. 53, nos. 3–4, pp. 265–275, Mar. 2020, doi: [10.1177/0020294019858217](https://doi.org/10.1177/0020294019858217).
- [8] J. Li, Q. Hu, and M. Ai, "Point cloud registration based on one-point RANSAC and scale-annealing biweight estimation," *IEEE Trans. Geosci. Remote Sens.*, vol. 59, no. 11, pp. 9716–9729, Nov. 2021, doi: [10.1109/TGRS.2020.3045456](https://doi.org/10.1109/TGRS.2020.3045456).
- [9] X. Shi, T. Liu, and X. Han, "Improved iterative closest point(ICP) 3D point cloud registration algorithm based on point cloud filtering and adaptive fireworks for coarse registration," *Int. J. Remote Sens.*, vol. 41, no. 8, pp. 3197–3220, Apr. 2020, doi: [10.1080/01431161.2019.1701211](https://doi.org/10.1080/01431161.2019.1701211).
- [10] F. A. Maken, F. Ramos, and L. Ott, "Stein ICP for uncertainty estimation in point cloud matching," *IEEE Robot. Autom. Lett.*, vol. 7, no. 2, pp. 1063–1070, Apr. 2022, doi: [10.1109/LRA.2021.3137503](https://doi.org/10.1109/LRA.2021.3137503).
- [11] I. Vizzo, T. Guadagnino, B. Mersch, L. Wiesmann, J. Behley, and C. Stachniss, "KISS-ICP: In defense of point-to-point ICP—Simple, accurate, and robust registration if done the right way," *IEEE Robot. Autom. Lett.*, vol. 8, no. 2, pp. 1029–1036, Feb. 2023, doi: [10.1109/LRA.2023.3236571](https://doi.org/10.1109/LRA.2023.3236571).
- [12] M. Brossard, S. Bonnabel, and A. Barrau, "A new approach to 3D ICP covariance estimation," *IEEE Robot. Autom. Lett.*, vol. 5, no. 2, pp. 744–751, Apr. 2020, doi: [10.1109/LRA.2020.2965391](https://doi.org/10.1109/LRA.2020.2965391).
- [13] C. Lin, C. Lin, and C. Chang, "An improved ICP with heuristic initial pose for point cloud alignment," *J. Internet Technol.*, vol. 21, no. 4, pp. 1181–1188, Jul. 2020, doi: [10.3966/160792642020072104026](https://doi.org/10.3966/160792642020072104026).
- [14] X. Yin, Y. Wang, Y. Chen, C. Jin, and J. Du, "Development of autonomous navigation controller for agricultural vehicles," *Int. J. Agricult. Biol. Eng.*, vol. 13, no. 4, pp. 70–76, Apr. 2020, doi: [10.25165/j.ijabe.20201304.5470](https://doi.org/10.25165/j.ijabe.20201304.5470).
- [15] P. Chhikara, R. Tekchandani, N. Kumar, V. Chamola, and M. Guizani, "DCNN-GA: A deep neural net architecture for navigation of UAV in indoor environment," *IEEE Internet Things J.*, vol. 8, no. 6, pp. 4448–4460, Mar. 2021, doi: [10.1109/JIOT.2020.3027095](https://doi.org/10.1109/JIOT.2020.3027095).
- [16] F. Rovira-Más, V. Saiz-Rubio, and A. Cuenca-Cuenca, "Augmented perception for agricultural robots navigation," *IEEE Sensors J.*, vol. 21, no. 10, pp. 11712–11727, May 2021, doi: [10.1109/JSEN.2020.3016081](https://doi.org/10.1109/JSEN.2020.3016081).
- [17] M. Reger, J. Stumpfenhausen, and H. Bernhardt, "Evaluation of LiDAR for the free navigation in agriculture," *AgriEngineering*, vol. 4, no. 2, pp. 489–506, Jun. 2022, doi: [10.3390/agriengineering4020033](https://doi.org/10.3390/agriengineering4020033).
- [18] S. Gunturu, A. Munir, H. Ullah, S. Welch, and D. Flippo, "A spatial AI-based agricultural robotic platform for wheat detection and collision avoidance," *AI*, vol. 3, no. 3, pp. 719–738, Aug. 2022, doi: [10.3390/ai3030042](https://doi.org/10.3390/ai3030042).
- [19] J. Neil, L. Cosart, and G. Zampetti, "Precise timing for vehicle navigation in the smart city: An overview," *IEEE Commun. Mag.*, vol. 58, no. 4, pp. 54–59, Apr. 2020, doi: [10.1109/MCOM.001.1900596](https://doi.org/10.1109/MCOM.001.1900596).
- [20] W. Liu, Z. Li, S. Sun, M. K. Gupta, H. Du, R. Malekian, M. A. Sotelo, and W. Li, "Design a novel target to improve positioning accuracy of autonomous vehicular navigation system in GPS denied environments," *IEEE Trans. Ind. Informat.*, vol. 17, no. 11, pp. 7575–7588, Nov. 2021, doi: [10.1109/THI.2021.3052529](https://doi.org/10.1109/THI.2021.3052529).
- [21] L. Yao, D. Hu, C. Zhao, Z. Yang, and Z. Zhang, "Wireless positioning and path tracking for a mobile platform in greenhouse," *Int. J. Agricult. Biol. Eng.*, vol. 14, no. 1, pp. 216–223, Jan. 2021, doi: [10.25165/j.ijabe.20211401.5627](https://doi.org/10.25165/j.ijabe.20211401.5627).
- [22] L. Song, H. Wang, and P. Chen, "Automatic patrol and inspection method for machinery diagnosis robot—Sound signal-based fuzzy search approach," *IEEE Sensors J.*, vol. 20, no. 15, pp. 8276–8286, Aug. 2020, doi: [10.1109/JSEN.2020.2978396](https://doi.org/10.1109/JSEN.2020.2978396).
- [23] S. D. Morad, R. Mecca, R. P. K. Poudel, S. Liwicki, and R. Cipolla, "Embodied visual navigation with automatic curriculum learning in real environments," *IEEE Robot. Autom. Lett.*, vol. 6, no. 2, pp. 683–690, Apr. 2021, doi: [10.1109/LRA.2020.3048662](https://doi.org/10.1109/LRA.2020.3048662).
- [24] O. S. Oubbati, M. Atiquzzaman, P. Lorenz, A. Baz, and H. Alhakami, "SEARCH: An SDN-enabled approach for vehicle path-planning," *IEEE Trans. Veh. Technol.*, vol. 69, no. 12, pp. 14523–14536, Dec. 2020, doi: [10.1109/TVT.2020.3043306](https://doi.org/10.1109/TVT.2020.3043306).
- [25] J. Tang, S. Lao, and Y. Wan, "Systematic review of collision-avoidance approaches for unmanned aerial vehicles," *IEEE Syst. J.*, vol. 16, no. 3, pp. 4356–4367, Sep. 2022, doi: [10.1109/JSYST.2021.3101283](https://doi.org/10.1109/JSYST.2021.3101283).
- [26] X. Ji, X. Wei, A. Wang, B. Cui, and Q. Song, "A novel composite adaptive terminal sliding mode controller for farm vehicles lateral path tracking control," *Nonlinear Dyn.*, vol. 110, no. 3, pp. 2415–2428, Nov. 2022, doi: [10.1007/s11071-022-07730-x](https://doi.org/10.1007/s11071-022-07730-x).
- [27] J. Zhang, Y. Yao, and B. Deng, "Fast and robust iterative closest point," *IEEE Trans. Pattern Anal. Mach. Intell.*, vol. 44, no. 7, pp. 3450–3466, Jul. 2022, doi: [10.1109/TPAMI.2021.3054619](https://doi.org/10.1109/TPAMI.2021.3054619).

- [28] R. Yang, Q. Li, W. Zhou, S. Yu, and J. Liu, "Speciation analysis of selenium nanoparticles and inorganic selenium species by dual-cloud point extraction and ICP-MS determination," *Anal. Chem.*, vol. 94, no. 47, pp. 16328–16336, Nov. 2022, doi: 10.1021/acs.analchem.2c03018.
- [29] X. Yue, Z. Liu, J. Zhu, X. Gao, B. Yang, and Y. Tian, "Coarse-fine point cloud registration based on local point-pair features and the iterative closest point algorithm," *Int. J. Speech Technol.*, vol. 52, no. 11, pp. 12569–12583, Feb. 2022, doi: 10.1007/s10489-022-03201-3.
- [30] F. Shi, T. Zhang, and T. Zhang, "Orientation-aware vehicle detection in aerial images via an anchor-free object detection approach," *IEEE Trans. Geosci. Remote Sens.*, vol. 59, no. 6, pp. 5221–5233, Jun. 2021, doi: 10.1109/TGRS.2020.3011418.
- [31] P. P. Groumpos, "A critical historic overview of artificial intelligence: Issues, challenges, opportunities, and threats," *Artif. Intell. Appl.*, vol. 1, no. 4, pp. 197–213, Oct. 2023.
- [32] K. Bhosle and V. Musande, "Evaluation of deep learning CNN model for recognition of devanagari digit," *Artif. Intell. Appl.*, vol. 1, no. 2, pp. 114–118, Feb. 2023, doi: 10.47852/bonviewia3202441.
- [33] W. Winterhalter, F. Fleckenstein, C. Dornhege, and W. Burgard, "Localization for precision navigation in agricultural fields—Beyond crop row following," *J. Field Robot.*, vol. 38, no. 3, pp. 429–451, May 2021, doi: 10.1002/rob.21995.
- [34] Q. Zhang, Q. Chen, Z. Xu, T. Zhang, and X. Niu, "Evaluating the navigation performance of multi-information integration based on low-end inertial sensors for precision agriculture," *Precis. Agricult.*, vol. 22, no. 3, pp. 627–646, Jun. 2021, doi: 10.1007/s11119-020-09747-x.
- [35] Z. Zhang, P. Li, S. Zhao, Z. Lv, F. Du, and Y. An, "An adaptive vision navigation algorithm in agricultural IoT system for smart agricultural robots," *Comput., Mater. Continua*, vol. 66, no. 1, pp. 1043–1056, Jul. 2020, doi: 10.32604/cmc.2020.012517.



NING XU was born in May 1983. She received the bachelor's degree in mechanical engineering and automation and the master's degree in mechanical engineering from Shandong Jianzhu University, in 2006 and 2015, respectively. She is currently pursuing the Ph.D. degree in agricultural engineering with Shandong University of Technology.

From 2006 to 2009, she was a Technical Engineer with China National Heavy Duty Truck Group Jining Commercial Vehicle Company Ltd.

From 2009 to 2024, she was the Deputy Director with the Field Equipment Research and Development Center, Shandong Academy of Agricultural Machinery Science. She was a Young Backbone Expert with Huang Huai Hai Key Laboratory of Modern Agricultural Equipment, Ministry of Agriculture and Rural Affairs. Mainly engaged in the research work of intelligent and information technology of agricultural equipment, focusing on the key technologies of unmanned operation, such as power transmission, path planning, and remote communication. In the past five years, she has presided more than or participated in 16 national and provincial-level scientific research projects, and published more than 20 related research articles, including six SCI/EI articles and more than 20 patents granted by the first or main inventor, software copyright more than ten items, participated in the publication of two books, *Apple Standard Orchard Production Mechanization Technology*, and *Agricultural Machinery Operation Information Technology Application Research*. She has won six science and technology awards (the first four), and the "Orchard Crawler Multi-Function Machine" has won the first prize in the 2021 Shandong Science and Technology Innovation Competition (rank 1/10).



ZHIHE LI was born in January 1975. Since 2014, he has been a President and a Professor of agricultural engineering with the College of Agricultural Engineering and Food Science, Shandong University of Technology. He is a Supervisor for master's students, doctoral candidates, and postdoctoral researchers. He presided more than the completion of two national 863 Program projects, the National Natural Science Foundation of China and Shandong Natural Science Foundation of China.

He has won six provincial-level science and technology awards, published more than 80 SCI/EI articles, and obtained 16 authorized invention patents.



JIANMING KANG was born in July 1984. He received the Ph.D. degree. He is currently a Researcher and the Vice President of Shandong Academy of Agricultural Machinery Science, the Deputy Director of Huang Huai Hai Key Laboratory of Modern Agricultural Equipment, Ministry of Agriculture and Rural Affairs, and a Master Supervisor with the College of Agricultural Engineering and Food Science, Shandong University of Technology. In 2018, get the "Young Top Talent"

title by Shandong Academy of Agricultural Machinery Sciences. In recent years, mainly engaged in orchard mechanization technology and equipment of the application of research and promotion. To preside more than and participate in ten scientific research projects at the provincial or ministerial level and above, and to apply for 26 patents (eight invention patents) by the first or main inventor, published 28 articles in domestic and foreign journals (12 included in EI). He won six provincial and the Ministerial Science and Technology Awards.



QINGSHAN MENG was born in May 1985. He received the bachelor's degree in software engineering from East China Jiaotong University, in 2016. He was a Young Backbone Expert in field equipment center with Shandong Academy of Agricultural Machinery Sciences and Huang Huai Hai Key Laboratory of Modern Agricultural Equipment, Ministry of Agriculture and Rural Affairs. Mainly engaged in the development of intelligent networking agricultural machinery

software system, presided more than or participated in more than ten provincial-level scientific research projects, published more than ten articles, the first or main inventor authorized more than ten patents, software copyright five, and participate in editing book *Apple Standard Orchard Production Mechanization Technology*.



MENGMENG NIU received the master's degree in mechanised agriculture engineering from South China Agricultural University, in 2016. He was a Young Backbone Expert in field equipment center with Shandong Academy of Agricultural Machinery Sciences and Huang Huai Hai Key Laboratory of Modern Agricultural Equipment, Ministry of Agriculture and Rural Affairs. Mainly engaged in green and efficient field management technology and equipment research. Presided more than or

participated in many national and provincial research projects, published more than 20 articles combined with related research, including seven SCI/EI, the first or main inventor to license more than 20 patents, software copyright seven.

...